Computed Effects of Solidity on Wells Turbine Performance*

J. K. WATTERSON** and S. RAGHUNATHAN**

The Wells turbine is one element in a chain of devices by which the oceans' wave power resource can be tapped. This paper reports a study of the performance and aerodynamics of a Wells turbine using a three-dimensional, flow solver for the Reynolds-averaged Navier-Stokes equations. Calculations have been performed for a monoplane device comprised of NACA 0015 blades under the conditions: Reynolds number 8×10^5, tip Mach number 0.4, hub-to-tip ratio 0.6 and tip clearance 2%. To study the effect of solidity calculations were performed for different numbers of blades. It is shown that the predicted effect of solidity on the turbine pressure drop, torque and efficiency agrees qualitatively and quantitatively with experimental data. The discrepancies can be partly explained by geometric differences between the experimental and numerical turbines. It is also shown that increasing turbine solidity increases the resistance to stall by strengthening the blade-to-blade interactions in the hub region.

Key Words: Fluids Engineering, Renewable Energy, Wave Power, Wells Turbine, Solidity, Computational Fluid Dynamics, Unstructured Meshes

1. Introduction

The energy resource contained in the swell of the world's oceans is an alternative to fossil fuels, which, if it can be harnessed both economically and with minimum environmental impact, is particularly attractive to small, remote coastal communities. The western coastlines of Great Britain and Ireland exposed to the North Atlantic Ocean are particularly well placed to harvest this resource, and it is estimated that the annual average wave power in this region is of the order of 120 GW[1]. The United Kingdom, which has a large coastline and number of isolated coastal or island-based communities, took an active interest in wave power about two decades ago, setting up nationally co-ordinated research activities at several establishments, one of which was at the Queen's University of Belfast (QUB). Of the several devices investigated, one of the most successful methods for wave power conversion was that based on the principle of an oscillating water column (OWC). This device operates on the principle that the hydraulic energy stored in the rise and fall of wave motion can be converted into pneumatic energy in an air column in a collecting chamber. The energy from this bi-directional air flow is then converted into mechanical energy by means of a Wells turbine (Fig. 1), which in its simplest form comprises a number of symmetrical aerofoil blades positioned around a hub with their chord planes normal to the axis of rotation. Finally, the turbine drives an electrical generator. The QUB research team designed and constructed a OWC/Wells turbine device on the island of Islay off western Scotland[2], and this has provided a rich source of further research of a multi-disciplinary nature including civil, electrical, mechanical and aeronautical engineering. This paper is concerned with the aerodynamics of the Wells turbine.

The pressure drop across a monoplane Wells turbine is proportional to the rotor tip speed and has a limit if transonic effects are to be avoided. When the collecting chamber is designed for wave amplitudes which generate a pressure drop greater than that which can be absorbed by the turbine without entering the transonic regime, it is common to resort to designs with multiple blades (without guide vanes) or multiple stages (with guide vanes)[3].

* Received 13th July, 1997
** Department of Aeronautical Engineering, The Queen's University of Belfast, Stranmillis Road, Belfast BT9 5AG, United Kingdom

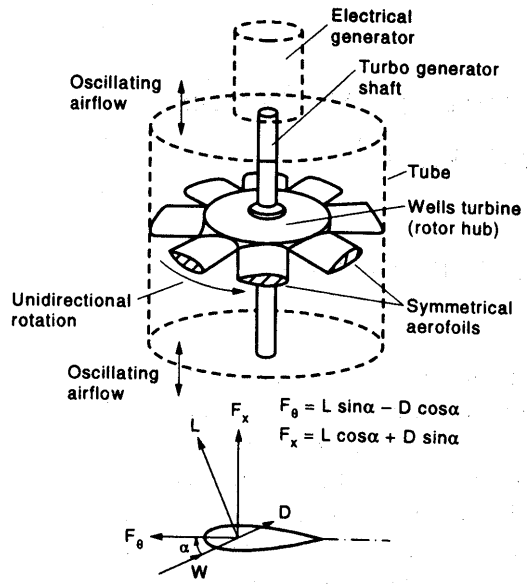

Fig. 1 Schematic of Wells turbine

The design methods generally used for predicting the performance of axial flow turbomachines have been used to predict the performance of the Wells turbine. These include the through-flow method, actuator disk theory and the Martensen method[4]. Typically, the rotor is divided into several annular rings, each ring being treated as a two-dimensional cascade, and since the rotational frequency of the blade disk is of the order of 100 Hz, whilst the frequency of the oscillation of the air flow is typically of the order of 0.1 Hz or less, the flow through the rotor is assumed to be quasi-steady. These methods are fast and efficient, and since they rely on data bases of experimental results, they are good design tools. However, they are not able to provide detailed descriptions of the flow, e.g. they cannot describe three-dimensional features such as the spanwise transport of stalled flow.

Computational Fluid Dynamics (CFD) provides a complementary method for studying the aerodynamic performance of the Wells turbine[5]; but like all tools, CFD is suitable for some, but not all purposes. The strength of CFD is that it allows a fuller investigation of the flow field than is possible with either experiments or the design methods described above; and it is particularly useful when used to aid the interpretation of experimental results. For example, very often, for reasons of expense, experiments have to be performed at low Reynolds numbers, and full-scale Reynolds number calculations can provide insight into the Reynolds number effects which may be present in the experiments. Moreover, CFD can be used to study the effect of such three-dimensional features as the tip clearance flow and hub and casing treatments which lie outside the ability of the simpler predictive tools to investigate.

This paper describes the use of a Reynolds-averaged Navier-Stokes CFD method to investigate the performance of a Wells turbine. The method employs an unstructured mesh which will eventually allow inclusion of such features as the blade tip and casing treatments, and multiple blade row interactions. Here, however, a typical monoplane turbine is modelled, allowing an investigation of the competence of the numerical method to be performed. Preliminary studies[6],[7] have shown that the numerical method is able to predict with reasonable accuracy the variations of pressure drop across the turbine disk and efficiency with flow coefficient, and the effect of tip clearance. Here we extend these studies to the effect of solidity on the performance of the turbine.

Nomenclature

C_T : torque coefficient
D_h : diameter at hub
D_t : diameter at casing
h : hub to tip ratio D_h/D_t
h_0 : stagnation enthalpy per unit mass
$\dot{m}$: mass flow rate
N : number of blades in annulus
$\dot{Q}$: volume flow rate
Q_R : volume flow rate ratio
R_t : tip radius of turbine
T : torque
U_t : blade tip velocity
V_x : axial velocity
$\Delta p, \Delta p^*$: static pressure drop and normalised pressure drop
η : efficiency
ϕ : flow coefficient
θ : tangential co-ordinate
σ : turbine solidity
τ_C : blade clearance at tip
Ω : angular velocity of turbine

2. Numerical Method

The numerical method used in this study is the unstructured mesh method of Dawes[8]-[10], called NEWT. The method was originally developed with turbomachinery applications in mind and has been successfully used in the study of a large number of turbomachinery flows, for example: heat transfer in the serpentine coolant passage of a turbine blade and interaction of the coolant gas with the primary flow[8]; unsteady rotor/stator interactions[9]; and influence of casing treatment on fan performance[10].

The equations solved are the fully three-dimensional, unsteady, Reynolds-averaged Navier-Stokes

equations, expressed in strong conservation form. Turbulence closure is provided by the k-ε model together with a modification of the low-Reynolds number model of Lam and Bremhorst[11] to handle the near wall regions. The seven equations of motion are cast in the absolute frame and are solved using the finite volume method of Jameson and Baker[12] in which the net flux imbalance into each cell is used to update the flow field variables at the nodes, using four stage Runge-Kutta time integration. The method is formally time accurate and can be used for calculating unsteady flows: though maximum local time steps are used to enhance the convergence of the solution procedure when steady state solutions are sought.

The primary control volumes are tetrahedral cells, and variables are stored at the vertices. Assuming a piecewise linear variation of variables over the faces of the cells, a second order accurate discretization of the convective flux terms is achieved. The viscous stresses are calculated for each cell and are assumed to be piecewise constant over cells. The viscous fluxes can then be estimated for the nodes of the mesh using Gauss's divergence theorem. Because a spatially centred discretisation is used, artificial dissipation is added to control solution decoupling and shock capture. The smoothing consists of a blend of second and fourth order differences; the fourth order terms operate throughout the solution domain and the second order terms are adaptively switched on only in the presence of high pressure gradients. Provided the mesh file is correctly configured, any three-dimensional tetrahedral mesh generator can supply the mesh for the flow solver. This work used the code's default mode which employs a simple H-mesh generator to create a baseline structured mesh of hexahedra. Each hexahedron is divided into six tetrahedra to form the unstructured mesh. This mesh retains the appearance of structure but does not inhibit the mesh refinement process (mesh refinement was not used in this work).

3. Calculations

3.1 Computational domain

The geometry chosen for these calculations is summarized below in Table 1. The blade is of constant, untwisted section and is set with its mid-chord-line aligned with a radius from the axis of rotation, giving the leading edge effective sweep back. The domain is extended 3.2 chord lengths upstream and downstream from the blade annulus; and is restricted to one blade-to-blade passage, with periodic boundaries. With a rotational speed, Ω, of 524 rad/s (equivalent to 5 000 rpm), the tip Mach number is 0.4, and the Reynolds number based on chord and relative tip speed is 8×10^5. Calculations were performed for 4, 6 and 8 blades, giving solidities of 0.32, 0.48 and 0.64 respectively.

Table 1 Modelled turbine

Aerofoil section	NACA0015
Number of planes	1
Number of blades N	4(0.32), 6(0.48), 8(0.64)
Tip Diameter D_t	0.5 m
Hub to tip ratio h	0.6
Tip clearance	2.0%
Rotational speed	5000 rpm
Tip Mach number	0.4
Reynolds number	8×10^5

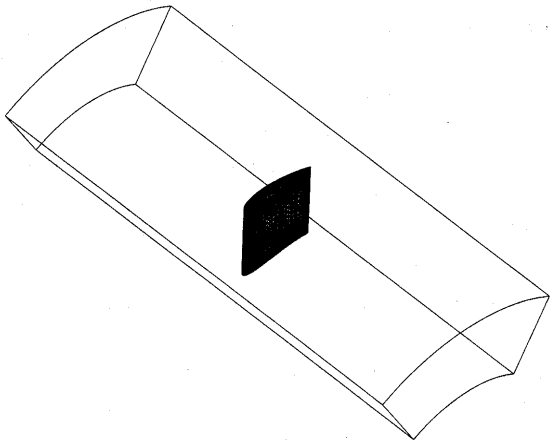

Fig. 2(a) Perspective view of computational domain showing mesh on turbine blade

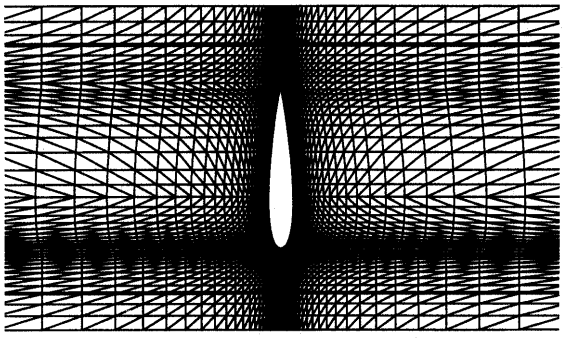

Fig. 2(b) Mesh about the blade at mid-span

3.2 The mesh

The mesh employed is illustrated in Fig. 2 (for $N=6$). Figure 2(a) shows a perspective view of the computational domain. The mesh in the centre of this figure is wrapped around the blade. Figure 2(b) shows the mesh on a surface of constant radius at mid-span in the vicinity of the blade.

As already stated, the tetrahedral mesh used for these calculations was developed from an H-mesh of hexahedra. The initial mesh comprised 71 nodes in the axial direction by 65 in the blade-to-blade (or tangential) direction by 33 in the spanwise direction. The blade leading and trailing edges were located at

the 26th and 55th blade-to-blade nodes, respectively. The radial variation of mesh in the region of the casing was chosen so that there were 3 cells across the tip clearance gap. After tetrahedralization the mesh contained 146 855 nodes and 823 884 cells.

3.3 Boundary conditions

At the inflow boundary the total temperature and velocity are specified. Static pressure is extrapolated and density and total internal energy are calculated. Inflow values of turbulent kinetic energy k and dissipation rate ε are also specified; in particular the turbulence level is 1% of the reference flow speed.

At the outflow boundary static pressure is specified. For these calculations an estimate of the exit swirl was made so that a radial static pressure distribution could be set. Density, velocity and the turbulence quantities are extrapolated and total internal energy is calculated.

The hub, casing and blade tip are treated as inviscid surfaces. The blade surface is treated as viscous. Wall functions are used to estimate the skin friction and the wall values of k and ε wherever the y^+ value of the node adjacent to the wall is greater than 10.

3.4 Calculated conditions

For each geometry calculations have been performed for several values of flow coefficient. The flow coefficient is defined as the ratio of the average inlet axial velocity to the tangential blade tip speed,

$$\phi=\frac{V_x}{U_t} \tag{1}$$

The values of flow coefficient used were 0.08, 0.10, 0.12 and 0.15.

4. Discussion

4.1 Turbine performance

It is first necessary to show that the numerical method is able to predict the performance of the turbine with reasonable accuracy. Experimental data is available from Gato and Falcao[13] for a very similar set of turbines, and this will be used for comparison with the predictions. A summary of the geometries studied in the experiments of Gato and Falcao is given below in Table 2.

Three performance parameters will be used in the comparison: pressure drop, Δp^*, torque coefficient C_T and efficiency, η. Pressure drop is defined as the change in volume averaged static pressure across the turbine (p_1-p_2), non-dimensionalised with respect to twice the tip relative dynamic head:

$$\Delta p^*=\frac{p_1-p_2}{\rho\Omega^2R_t^2} \tag{2}$$

where R_t is the tip radius. The torque coefficient is obtained by non-dimensionalising the turbine torque

Table 2 Experimental turbines of Gato and Falcao[13]

Aerofoil section	NACA0012
Number of planes	1
Number of blades N	4(0.29), 6(0.44), 8(0.59)
Tip Diameter D_t	0.6 m
Hub to tip ratio h	0.5
Tip clearance	1%
Rotational speed	2700 rpm
Tip Mach number	0.25
Reynolds number	5.6×10^5

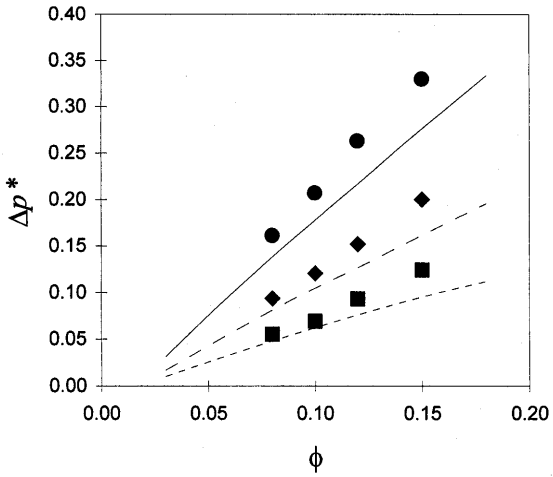

Fig. 3 Variation of pressure drop with flow coefficient
Measured: ---$N=4$, $\sigma=0.29$; – – –$N=6$, $\sigma=0.44$; ——$N=8$, $\sigma=0.59$
Computed: ■ $N=4$, $\sigma=0.32$; ◆ $N=6$, $\sigma=0.48$; ●$N=8$, $\sigma=0.64$

with respect to $\rho\Omega^2R_t^5$, i.e.

$$C_T=\frac{T}{\rho\Omega^2R_t^5} \tag{3}$$

Efficiency is usually defined as the useful work done by the turbine divided by the change in total enthalpy:

$$\eta=\frac{T\Omega}{\dot{m}(h_{01}-h_{02})} \tag{4}$$

where T is the torque, $\dot{m}$ is the mass flow rate and h_{01} and h_{02} are, respectively, the inflow and outflow total enthalpies per unit mass. However, the drop in stagnation enthalpy is very small compared to h_{01} and h_{02}, and for consistency with the experimental results given in Ref.(13), the efficiency used here is defined as the useful work done divided by the product of the volume flow rate and the drop in static pressure across the turbine.

$$\eta=\frac{T\Omega}{\dot{Q}(p_1-p_2)} \tag{5}$$

Measured and predicted values of the pressure drop are compared in Fig. 3. The comparison is good. Qualitatively, the predicted variations of pressure drop with flow coefficient are almost linear, as expected. The predicted effect of increasing solidity is to increase the pressure drop at any given value of ϕ, also as expected. Quantitatively, the slopes of the

predicted performance curves are higher than the corresponding measurements. The maximum error in Δp^* is about 22% and the average error is about 15%. In part, the discrepancy may be explained by five factors. First, the experiments were performed at a lower tip Mach number than the calculations. The Prandtl-Glauret correction factor for geometrically identical blades would be $\sqrt{(1-0.25^2)/(1-0.40^2)}=1.06$. Second, the experiments used a NACA 0012 profile while the calculations were performed for NACA 0015 blades. Reference (14) quotes a lower lift curve slope for the thicker profile, giving a thickness correction factor of 0.96. Third, the solidity of the experimental turbines is lower than the corresponding analysed turbines. The difference is about 10%, and since Δp^* rises more rapidly than linearly with σ, a correction factor of 1.15 is justifiable from the data. Fourthly, increasing the tip clearance from 1% to 2% may reduce the pressure drop by as much as 6%[7]. Finally, the calculations assume that there are no boundary layers on the hub or casing, so that these regions of the analysed turbines will be operating at higher angles of incidence than the corresponding experimental turbines. It is difficult to put a number on this correction, so we will assume a factor of just 1.0. Putting these factors together gives an overall correction of 1.10, which is not far off the average difference of 15% already noted.

Similar comments can be made about the comparison between measured and predicted torque coefficients, shown in Fig. 4. Both the qualitative and quantitative trends with respect to ϕ and σ are correct. Again the predicted values are slightly higher than the measured ones, though the error is smaller in this case. This is probably due to the smaller tip clearance of the experimental turbines, which has a more pronounced effect on torque than on pressure drop. Increasing the clearance from 1% to 2% can reduce the torque generated by about 10%[7].

Finally, the comparison between measured and predicted efficiencies is shown in Fig. 5. The calculations have been performed in the range of ϕ which gives maximum efficiency, and so do not exhibit the rapid rise which occurs at low values of ϕ when the blade leading edge thrust increases more quickly than the viscous drag. Neither have the calculations been taken to the point of stall, shown by the cut-off of the experimental curves. The general level of the predicted efficiencies is too high. Combining Eqs.(2), (3) and (5) gives

$$\eta=\left(\frac{C_T}{\Delta p^*}\right)\left(\frac{\Omega R_t^3}{\dot{Q}}\right) \qquad (6)$$

This implies that the predicted values of the volume flow rate ratio $Q_R=\Omega R_t^3/\dot{Q}$ are too large. Assuming that the volume flow rate is used to calculate the mean axial velocity, it can be shown that the ratio of Q_{R1} for a machine with hub to tip ratio h_1 to Q_{R2} for a similar machine with hub to tip ratio h_2 at the same value of flow coefficient is given by

$$\frac{Q_{R1}}{Q_{R2}}=\frac{1-h_2^2}{1-h_1^2} \qquad (7)$$

The ratio for the analysed turbines (1) to the experimental turbines (2) is therefore $(1-0.5^2)/(1-0.6^2)=1.17$. This difference of 17% explains some of the difference in peak efficiency between the predictions and the measurements.

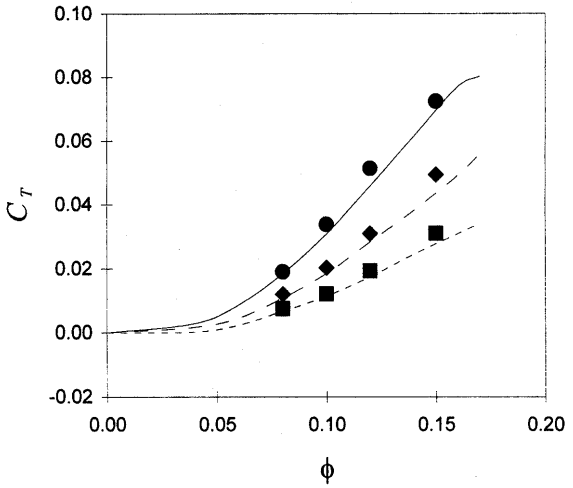

Fig. 4 Variation of torque coefficient with flow coefficient
Measured: ---$N=4$, $\sigma=0.29$; ———$N=6$, $\sigma=0.44$; ——$N=8$, $\sigma=0.59$
Computed: ■ $N=4$, $\sigma=0.32$; ◆ $N=6$, $\sigma=0.48$; ● $N=8$, $\sigma=0.64$

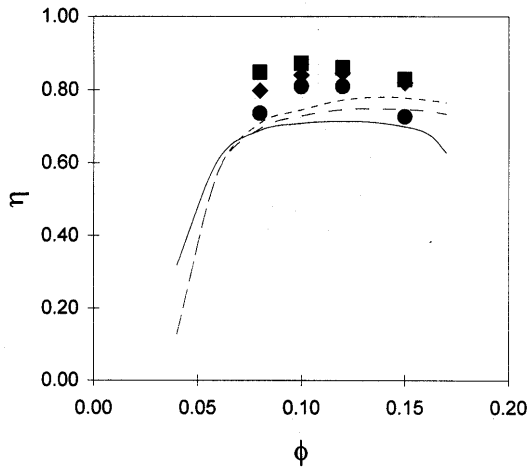

Fig. 5 Variation of efficiency with flow coefficient
Measured: ---$N=4$, $\sigma=0.29$; ———$N=6$, $\sigma=0.44$; ——$N=8$, $\sigma=0.59$
Computed: ■ $=4$, $\sigma=0.32$; ◆$N=6$, $\sigma=0.48$; ● $N=8$, $\sigma=0.64$

4.2 Turbine aerodynamics

An important aspect of the effect of solidity on the aerodynamics of the turbine is its influence on stall. The results published in Ref.(13) indicate that turbine stall occurred earliest for the lowest solidity turbine (at a flow coefficient just above 0.15), while the $\sigma=0.44$ and 0.59 turbines stalled, respectively, just before and just after $\phi=0.17$. A similar, qualitative observation concerning the influence of solidity on stall is made in Ref.(5).

Prediction of the flow coefficients at which the analysed turbines stall would be very difficult. However, qualitative information about the influence of solidity on the turbine aerodynamics can be gleaned from the calculations. Figure 6 shows the contours of Mach number just above the blade root for (a) $\sigma=0.32$ and (b) $\sigma=0.64$, both at $\phi=0.10$. Similarly, Fig. 7 shows the contours of Mach number just below the blade tip for (a) $\sigma=0.32$ and (b) $\sigma=0.64$, also at $\phi=0.10$. Considering Fig. 6 first, the higher solidity flow shows much stronger coupling between blade rows. The wake of the upstream blade interacts with the boundary layer developing on the downstream blade, and the boundary layer remains attached over the entire blade chord. In contrast, the lower solidity turbine shows a weaker interaction between upstream and downstream blades, and the boundary layer appears to separate at about 65% chord. The higher solidity turbine would also cause a stronger radial redistribution of the axial flow, reducing the local axial velocity and angle of incidence. A similar picture is seen in Fig. 7 at the blade tip. Here the contours are dominated by the clearance vortex. Again the inter-blade interaction is stronger in the higher solidity turbine.

The predicted velocity vectors just adjacent to the suction surfaces of the $\sigma=0.32$ and $\sigma=0.64$ turbines at $\phi=0.10$ are shown in Figs. 8(a) and 8(b), respectively. These show that while the flow is fully attached on the suction surface of the higher solidity turbine, there is a small region of reversed flow at the root of the lower solidity case.

Taking the evidence of Figs. 6 to 8 together indicates that increasing turbine solidity stabilises the flow at the blade root by (a) strengthening the viscous interaction between blades and (b) redistributing axial flow away from the hub region, thus decreasing the local blade incidence. This delays stall of the hub flow. Conversely, with low solidity the hub section will be at a higher angle of incidence and will, therefore, be inclined to stall at lower values of flow coefficient. Once the hub flow has stalled, the extra blockage causes radial redistribution of the flow, which in turn advances stall at higher radii.

(a) $\sigma=0.32$, $\phi=0.10$

(b) $\sigma=0.64$, $\phi=0.10$

Fig. 6 Mach contours just above blade root

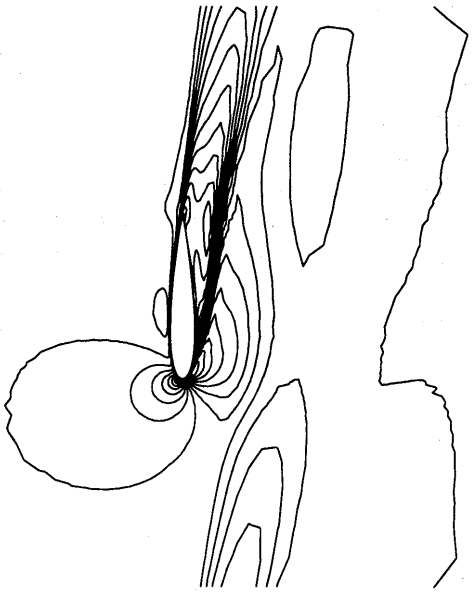

(a) $\sigma=0.32$, $\phi=0.10$

(b) $\sigma=0.64$, $\phi=0.10$

Fig. 7 Mach contours just below blade tip

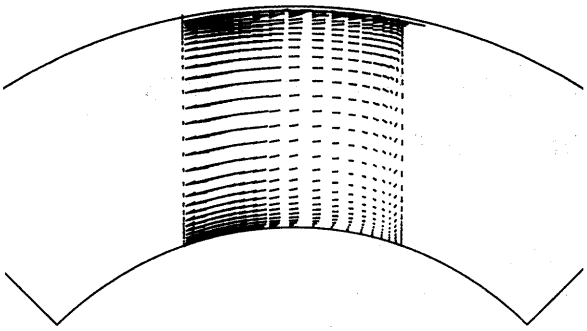

(a) $\sigma=0.32$, $\phi=0.10$

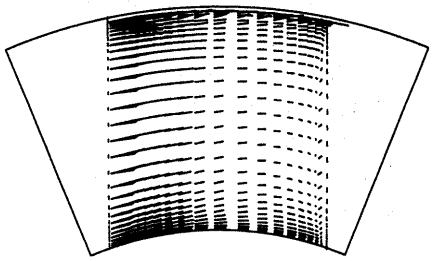

(b) $\sigma=0.64$, $\phi=0.10$

Fig. 8 Suction surface velocity vectors

5. Conclusions

The ability of an unstructured mesh CFD method to predict the effect of solidity on the performance of a monoplane Wells turbine has been tested. It has been shown that the method is able to predict the effect of solidity on the pressure drop characteristic of the turbine both qualitatively and quantitatively. The difference between the experimental measurements and the predictions could be explained in terms of the different tip Mach number and differences in geometry. Good qualitative and quantitative predictions of the effect of solidity on torque coefficient have also obtained. Efficiency is over predicted throughout the range of cases calculated, but some of the difference could be attributed to differences in geometry.

The calculations have also been used to help explain the effect of solidity on Wells turbine stall. As solidity is increased, the interaction between adjacent blades strengthens. At the blade root, the upstream blade wake mixes with the downstream suction surface boundary layer in a strong viscous interaction. The increased blockage of the flow at the blade root causes radial redistribution of the flow which reduces the axial component at the root, and hence reduces the angle of incidence. Lower solidity turbines experience less radial redistribution of the flow and are inclined to stall at lower flow coefficients.

Acknowledgement

The authors acknowledge and are grateful to Prof. W. N. Dawes for allowing the use of his CFD code in this work.

References

(1) Thorpe, T.W., A Review of Wave Energy, DTI Report ETSU-R-72, (1992).

(2) Whittaker, T.J.T., Shoreline Wave Power on the Isle of Islay (1990), Institute of Engineers and Shipbuilders in Scotland.

(3) Raghunathan, S., Setoguchi, S. and Kaneko, K., Mutliplane Wells Turbine for Wave Energy Conversion, First International Conference on Energy Conversion and Energy Sources Engineering (1990), Wuhan, China.

(4) Raghunathan, S., Aerodynamics of Cascades at a Stagger Angle of 90 degrees, 34th Aerospace Sciences Meeting and Exhibit, Reno, NV, Paper AIAA 96-0283, (1996).

(5) Raghunathan, S., The Wells Air Turbine for Energy Conversion, Progress in Aerospace Sciences, Vol. 31 (1995), p. 335-386.

(6) Watterson, J.K. and Raghunathan, S., Investigation of Wells Turbine Performance Using 3-D CFD, Proc. 31st Intersociety Energy Conversion Engineering Conference, (1996).

(7) Watterson, J.K. and Raghunathan, S., Computed Effects of Tip Clearance on Wells Turbine Performance, 35th Aerospace Sciences Meeting, AIAA 97-0994, Reno, (1997).

(8) Dawes, W.N., The Practical Application of Solution-Adaption to the Numerical Solution of Complex Turbomachinery Problems, Progress in Aerospace Sciences, Vol. 29 (1993), p. 221-269.

(9) Dawes, W.N., A Numerical Study of the Interaction of a Transonic Compressor Rotor Overtip Leakage Vortex with the Following Stator Blade Row, ASME-IGTI Conference, The Hague, Netherlands, Paper 94-GT-156, (1994).

(10) Aubert, S. and Dawes, W.N., Numerical Analysis of an Axial Flow Fan with Air-Separator Equipment, 31st AIAA/ASME/SAE/ASEE Joint Propulsion Conference and Exhibit, San Diego, CA, Paper AIAA 95-2341, (1995).

(11) Lam, C.K.G. and Bremhorst, K.A., Modified Form of the k-ε Model for Predicting Wall Turbulence, Journal of Fluids Engineering, Vol. 103 (1981), p. 456-460.

(12) Jameson, A. and Baker, T.J., Improvements to the Aircraft Euler Method, AIAA 25th Aeronautical Sciences Meeting, Paper AIAA 87-0452, (1987).

(13) Gato, L.M.C. and Falcao, A.F.DeO., Aerodynamics of the Wells Turbine, International Journal of Mechanical Sciences, Vol. 30, No. 6 (1988), p. 383-395.

(14) Abbott, I.A. and von Doenhoff, A.E., Theory of Wing Sections (1959), Dover Publications Inc., New York.